Supplementary Material

The microfluidic multitrap nanophysiometer for hematologic cancer cell characterization reveals temporal sensitivity of the calcein-AM efflux assay

Thomas F. Byrd IV[1,6], Loi T. Hoang[1], Eric G. Kim[1], Matthew E. Pfister[1], Erik M. Werner[1], Stephen E. Arndt[1], Jeffrey W. Chamberlain[1], Jacob J. Hughey[1], Bao A. Nguyen[1], Erik J. Schneibel[1], Laura L. Wertz[1], Jonathan S. Whitfield[3], John P. Wikswo[1,2,3,4,5], & Kevin T. Seale[1,2,3*]

[1]Searle Systems Biology and Bioengineering Undergraduate Research Experience, Vanderbilt University, Nashville, TN, 37235, USA, [2]Vanderbilt Institute for Integrative Biosystems Research and Education, Vanderbilt University, Nashville, TN, 37235, USA, [3]Department of Biomedical Engineering, Vanderbilt University, Nashville, TN, 37235, USA, [4]Department of Physics and Astronomy, Vanderbilt University, Nashville, TN, 37235, USA, [5]Department of Molecular Physiology and Biophysics, Vanderbilt University, Nashville, TN, 37232, USA, [6]University of New Mexico School of Medicine, Albuquerque, NM, 87131, USA.

[*]Correspondence should be addressed to K.T.S. (email: kevin.seale@vanderbilt.edu).

We present data that further demonstrate the capabilities of the multitrap nanophysiometer (MTNP).

Cell residence and cell division. We have used the MTNP to monitor the growth of different cell types in the MTNP on an automated, temperature-controlled microscopy platform to validate the system's microbiological compatibility. Individual Jurkat T cells perfused with conditioned media were able to successfully divide in the MTNP at 48.9 ± 5.2 hr intervals (Fig. S1a). *S. cerevisiae* cells budded in the MTNP at regular intervals of approximately 98 min (Fig. S1b), closely matching the interval for batch-cultured cells in our laboratory. In subsequent experiments with Jurkat cells we observed robust cell motion and

division over periods of several days in the presence of traditional cell viability indicators, a finding that is consistent with recent literature on microfluidic cell culture.[1]

Figure S1c illustrates 3.2 pL capacity MTNP traps loaded with live *S. cerevisiae*. The obstructed trap in the center, encircled in blue, initially contained only one or two yeast cells that grew quickly to fill the trap to capacity over a period of 6.5 hr. The inverse normalized mean integrated optical density (1 – IOD) in the growth region increases to a maximum and is reasonably well approximated by an exponential growth curve (Fig. S1d), assuming an initial trap volume fraction of 5% (one cell) and doubling time of 98 min. The trap reached capacity at approximately 400 min, which corresponds to 4.5 cell cycles and about 23 cells ($2^{4.5}$). This is close to the number of cells predicted by a simple volume calculation (21 cells) assuming a yeast radius of 3 μm and a packing fraction of 74%. When the 3.2 pL traps are full of growing yeast, the MTNP behaves much like a chemostat,[2] with a constant number of cells growing at a controllable rate. Each 3.2 pL trap brims with a tiny yeast colony in a constant state of log phase growth. Unlike a traditional chemostat, the flow of fresh media in the MTNP can be increased without increasing the washout of cells. This is advantageous in some circumstances, since cells can be maintained in fresh media without accumulation of cellular metabolic by-products. Large-scale yeast chemostats operate at cell fractions of 5-10%, while the MTNP operates near 15% cell fraction when every trap is full, which may help increase biomolecule concentration in the outlet stream. It is possible to design MTNPs with higher cell

fractions if desired. We have documented in detail elsewhere the use of optical tweezers in the MTNP.[3]

Methods – Cell residence and division. Methods for loading the MTNP with cells have been described in detail elsewhere.[4-6] Jurkat T cells were cultured in RPMI with 10% FBS and split every 2-3 days, according to standard ATCC culture methods. All cells used were below their ninth passage. The protocol for loading Jurkats was the same in all experiments. After perfusing device with media to remove all air bubbles, the PEEK tubing from the inlet was removed and placed in a suspension of cells diluted to $1x10^6$ cells per mL media. Flow was reversed at 200 nL min^{-1} for 5-10 min, depending on trap array size, to aspirate cells. Flow was again reversed in the forward direction as PEEK tubing was reinserted into its MTNP, allowing cell expiration and trapping at a flow rate that remained at 200 nL min^{-1} throughout the length of the experiment. *S. cerevisiae,* obtained from Dr. Carl Johnson's lab at Vanderbilt University, were loaded according to the same protocol but from a dilution of $3x10^6$ cells per mL of standard yeast media. Cells were retained for up to 72 hr with time-lapse bright field images taken once every 60 s.

The exponential yeast growth equation in Figure S1c was derived assuming a starting population of one *S. cerevisiae* cell. The x0 value of 0.05 at t=0 was used to represent this initial population and accordingly describes the fractional occupancy of a single yeast in the trap projected onto the 2D image of the entire square trap area. The 98 min doubling time represents the average time taken for a trapped *S. cerevisiae* cell to divide in the MTNP.

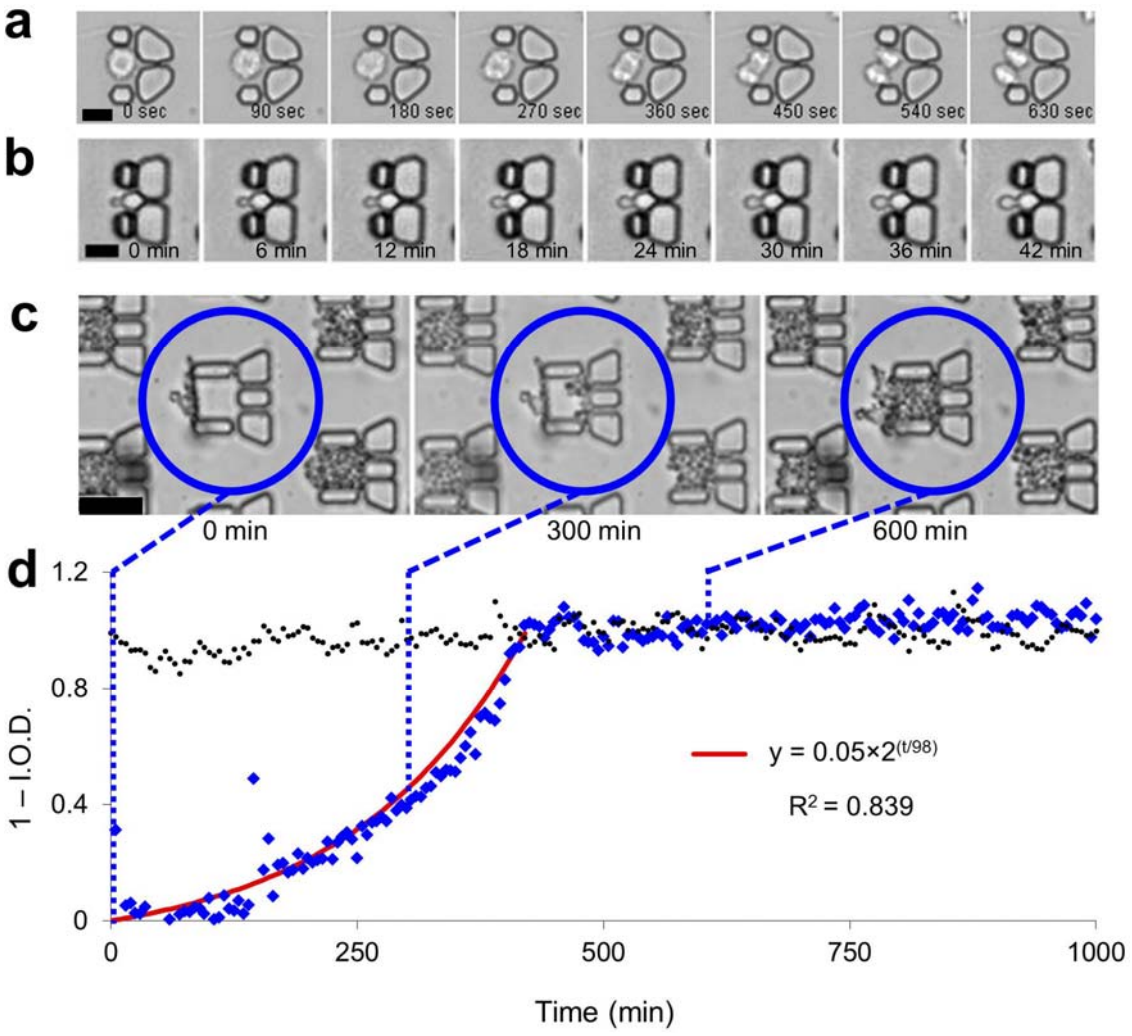

Figure S1 Cell division and growth in the MTNP. (**a**) Jurkat T cell division in a 3.0 pL capacity trap well. Scale bar, 15 µm. (**b**) Budding of a single *S. cerevisiae* cell trapped in a 300 fL pentagonal well. Scale bar, 10 µm. (c) Exponential growth of *S. cerevisiae* in a 3.2 pL occlusion-limited trap. Scale bar, 40 µm. (d) Inverse optical density (IOD) of traps as a function of time. The data were calculated from corresponding time-lapse images acquired 1 min apart. IOD values for the trap encircled above are shown in blue and resulted in the red exponential growth curve pictured. Black values were taken from an already-full trap imaged simultaneously in the same FOV as the encircled trap.

Membrane labeling of cells. We have additionally sought to approximate the concentrations and labeling times that enable detection of fluorescently conjugated antibodies bound to biomarkers on individual cells trapped within the MTNP using a microscope and cooled charge-coupled device (CCD) camera. CD45, a protein tyrosine phosphatase implicated in T cell antigen receptor signaling, is a specific target of traditional fluorescence-activated cell sorting (FACS) that is present in large quantities on the surface of Jurkat T cells. Figure S2 illustrates the fluorescence minus background of Jurkat cells in MTNP traps over time as allophycocyanin (APC) conjugated anti-CD45 antibody is introduced into the trap chamber. Three concentrations of anti-CD45 antibody were evaluated, and each produced a similar signal-to-noise ratio in fluorescence images of the labeled cells. At higher anti-CD45 antibody concentrations, the fluorescence signal plateaus after 30-40 min, which is most likely due to saturation of the finite number of membrane receptors. The slope of membrane fluorescence versus time was less and the time to plateau was greater for lower anti-CD45 antibody concentrations, as would be expected with a diffusion-limited process. Based on this information we modeled the receptor-ligand kinetics for anti-CD45 labeling using the differential equation

$$\frac{dC}{dt} = k_{on} L_f R_t - k_{on} L_f C - k_{off} C \,, \tag{1}$$

where the number of cellular CD45 receptors (R_t) is constant and free anti-CD45 ligand (L_f) is maintained at a constant level by the inflow. The receptor-ligand complex (C) is formed at a rate dC/dt that is proportional to the binding rate (k_{on}) and diminished by loss of available free receptors and by ligand disassociation

from receptors (k_{off}). The model was fit to the experimental data for L_f values of 1.9 µg mL^{-1}, 6.9 µg mL^{-1}, and 12.1 µg mL^{-1} using a Generalized Reduced Gradient method in Microsoft Excel and yielded values for $R_{tot,1.9}$ = 22.65 a.u., $R_{tot,6.9}$ = 22.40 a.u., $R_{tot,12.1}$ = 20.03 a.u., K_{on} = 5.73e-3 min^{-1} and k_{off} = 0.00 min^{-1}. Notably, the outline of the cells was apparent on the fluorescence images before saturation occurred, demonstrating that complete saturation is not necessary for membrane marker identification in the case of CD45. We have seen similar results with peridinin-chlorophyll protein complex (PerCP) anti-CD69 antibody and are conducting similar experiments with phycoerythrin conjugated anti-CD3 antibody and fluorescein isothiocyanate anti-CD19 antibody labels. The experimental layout above is easily modified with a fixation protocol to accommodate immunocytochemistry studies on intracellular protein production and localization.[7,8]

Methods – Membrane Labeling: Jurkat cells were loaded into the MTNP as described earlier and perfused with culture media containing allophycocyanin (APC) conjugated anti-CD45 antibody while bright field and fluorescence images were simultaneously collected every 30 s. Cell fluorescence over time was extracted using the methods described previously. Experiments were conducted using one of the following anti-CD45 concentrations: 1.9 µg mL^{-1}, 6.9 µg mL^{-1}, or 12.1 µg mL^{-1}.

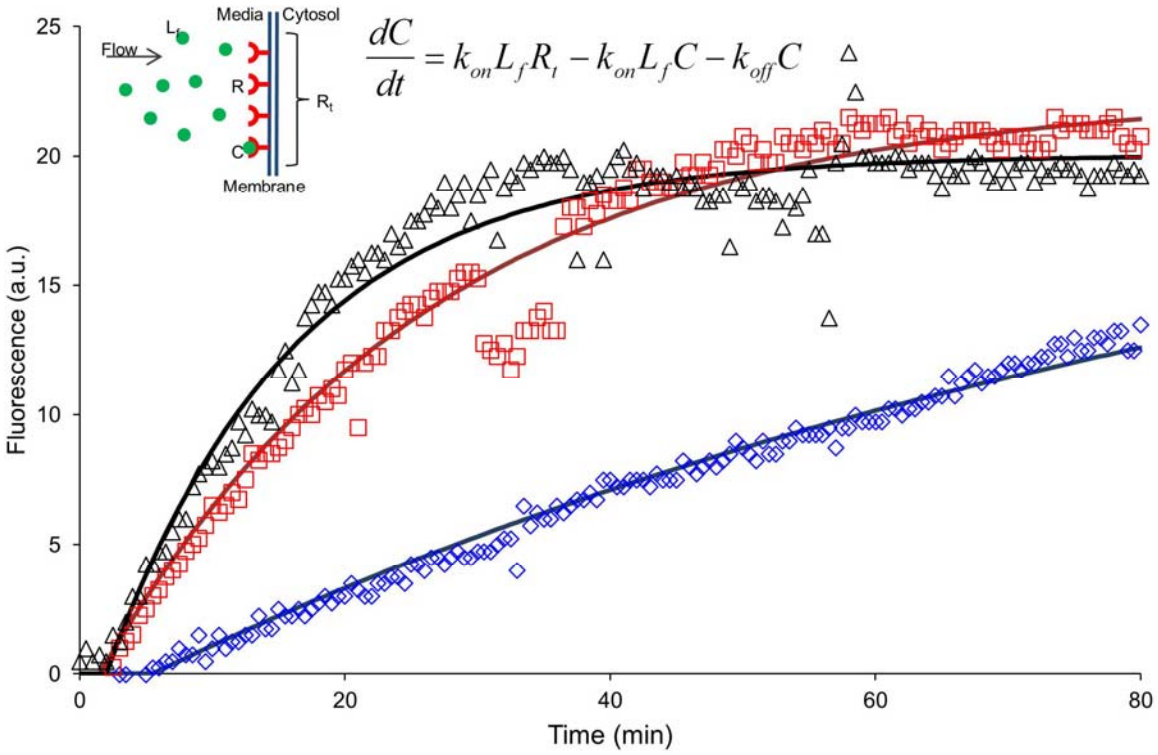

Figure S2. Labeling of membrane CD45 on live Jurkat T cells with fluorescent antibodies in the MTNP. The labeling results using three different anti-CD45 antibody concentrations are shown. Inset cartoon depicts the free anti-CD45 antibodies in the perfusing media (L_f) encountering the total number of CD45 receptors on a trapped cell's surface (R_t) and forming fluorescent receptor-antibody complexes (C) at the rate of dC/dt as described in the associated equation. The model assumes that the rate of C formation is diminished as the number of available CD45 receptors (R) decreases. Each plot is the average of four randomly selected traps from a field of view containing 200 traps. Data points were taken every 1 min and normalized to background illumination.

Pinocytic loading. We can deliberately introduce foreign molecules into the cytosol of Jurkat cells using a pinocytic loading (PL) method adapted for the MTNP, a cyclic process that results in cytosolic loading due to osmotic bursting of pinosomes.[9-11] Here we successfully loaded fluorescent dextrans of increasing size into Jurkat T cells by intra-microfluidic pinocytic loading. Figure S3 illustrates the pinocytic loading procedure schematically, with bright field and simultaneous fluorescence images of representative cells from the experiment. Using the MTNP, we have shown that intra-microfluidic pinocytic loading of 3,000 MW dextrans into cells performs with up to 30% greater efficiency than conventional PL techniques,[9] and we have successfully loaded fluorescent dextrans with molecular weights as high as 70,000 using the same methods (data not shown).

Methods – Pinocytic Loading. Jurkat cells were loaded into the MTNP as described earlier. Hypertonic media containing dextrans consisted of normal RPMI supplemented with 0.5 M sucrose and 10% polyethylene glycol (PEG) 1000. Hypotonic media consisted of RPMI diluted 6:4 with DI water. Hypertonic exposure for 10 min was followed by hypotonic exposure for 2 min.

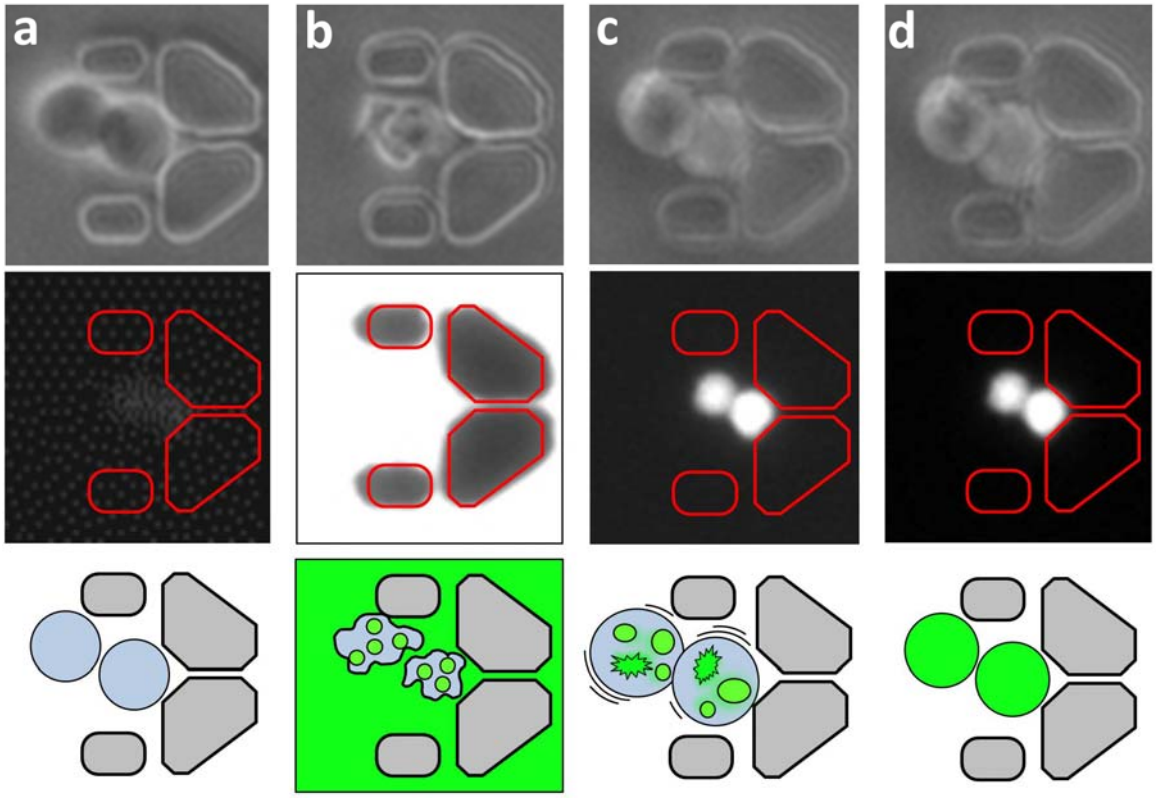

Figure S3 Pinocytic loading of FITC dextran in the MTNP. The top and middle rows show bright field and fluorescence images of 2 trapped Jurkat T cells being loaded with 3,000 MW fluorescent dextrans, respectively. The bottom row is a schematic illustration of the procedure. (**a**) Two cells at the beginning of the experiment. (**b**) The same cells during hypertonic media exposure, taking up fluorescent green dextran into pinosomes. Background brightness is caused by free fluorescent dextran in the media. (**c**) Pinosomes rupturing during hypotonic media exposure, releasing dextran load into the cytosol. (**d**) Return to normal media; cells now loaded with cytosolic fluorescent dextrans.

References

1. Wlodkowic, D. et al. Chip-based dynamic real-time quantification of drug-induced cytotoxicity in human tumor cells, *Anal. Chem.*, **81,** 6952-6959, 2009

2. Novick, A., Szilard, L. Description of the chemostat, *Science*, **112,** 715-716, 1950

3. Chowdhury, S. et al. Automated cell transport in optical tweezers-assisted microfluidic chambers, *IEEE T. Autom. Sci. Eng.*, **10,** 980-89, 2013

4. Faley, S. et al. Microfluidic platform for real-time signaling analysis of multiple single T cells in parallel, *Lab Chip*, **8,** 1700-1712, 2008

5. Faley, S. L. et al. Microfluidic single cell arrays to interrogate signalling dynamics of individual, patient-derived hematopoietic stem cells, *Lab Chip*, **9,** 2659-2664, 2009

6. Seale, K. T., Faley, S. L., Chamberlain, J., Wikswo, J. P., Jr. Macro to nano: A simple method for transporting cultured cells from milliliter scale to nanoliter scale, *Exp. Biol. Med.*, **235,** 777-783, 2010

7. Faley, S., Copland, M., Reboud, J., Cooper, J. M. Intracellular protein trafficking kinetics in chronic myeloid leukemia stem cells using a microfluidic platform, *Integr. Biol.*, **4,** 368-373, 2012

8. Faley, S. L., Copland, M., Reboud, J., Cooper, J. M. Cell chip array for microfluidic proteomics enabling rapid in situ assessment of intracellular protein phosphorylation, *Biomicrofluidics*, **5,** 024106, 2011

9. Hughey, J. J., Wikswo, J. P., Seale, K. T. Intra-microfluidic pinocytic loading of Jurkat T cells. In: *IEEE/NIH Life Science Systems and Applications Workshop*, IEEE, Piscataway, NY, 132-135, 2007

10. Okada, C. Y., Rechsteiner, M. Introduction of macromolecules into cultured mammalian-cells by osmotic lysis of pinocytic vesicles, *Cell*, **29,** 33-41, 1982

11. Gilmore, K. J., Quinn, H. E., Wilson, M. R. Pinocytic loading of cytochrome c into intact cells specifically induces caspase-dependent permeabilization of mitochondria: evidence for a cytochrome c feedback loop, *Cell. Death Differ.*, **8,** 631-639, 2001